GO-VIKING

Research and Innovation Action (RIA)

This project has received funding from the Euratom research and innovation programme 2021-2025 under Grant Agreement No 101059603

Start date : 2022-06-01 Duration : 48 Months

TREFLE experiment: presentation of the data

Authors : Dr. Daniele VIVALDI (IRSN)

GO-VIKING - Contract Number: 101059603

Project officer: Angelgiorgio IORIZZO

Document title	TREFLE experiment: presentation of the data
Author(s)	Dr. Daniele VIVALDI
Number of pages	25
Document type	Deliverable
Work Package	WP4
Document number	D4.3
Issued by	IRSN
Date of completion	2024-07-15 12:18:18
Dissemination level	Public

Summary

Description of the TREFLE two-phase FIV experiment and benchmark setup

Approval

Date	By
2024-07-15 13:07:26	Mr. William BENGUIGUI (EDF)
2024-07-15 13:09:49	Dr. Papukchiev ANGEL (GRS)

GO VIKING

TREFLE experiment: presentation of the data

Deliverable D4.3

Version N°1
May/2024

Antonio Chahine, Daniele Vivaldi (Institut de Radioprotection et de Sûreté Nucléaire (IRSN), Cadarache, St Paul-lez-Durance BP3, 13115, France)

Funded by
the European Union

Disclaimer

The content of this report reflects only the author's view. The European Commission is not responsible for any use that may be made of the information it contains.

Document information

Grant Agreement / Proposal ID	101060826
Project Title	Gathering expertise On Vibration ImpaKt In Nuclear power Generation
Project Acronym	GO-VIKING
Scientific Coordinator	Angel Papukchiev, mailto:angel.papukchiev@grs.de, GRS Kevin Zwijsen, mailto:zwijsen@nrg.eu, NRG
Project starting date (duration)	1st June 2022 – 31st May 2026 (48 Months)
Related Work Package	WP4
Related Task(s)	Task 4.3
Lead Organisation	Institut de Radioprotection et de Sûreté Nucléaire (IRSN)
Contributing Partner(s)	Institut de Radioprotection et de Sûreté Nucléaire (IRSN)
Due Date	
Submission Date	
Dissemination level	

History

Date	Version	Submitted by	Reviewed by	Comments
31.05.2024	1.0	IRSN		

Table of contents

List of figures

Funded by
the European Union

List of tables

Funded by
the European Union

Abbreviations and Acronyms

Acronym	description
WP	Work package
GO-VIKING	Gathering expertise On Vibration ImpaKt In Nuclear power Generation
TREFLE	Two-phase flow REgimes and FLuid structure-interaction Experimental facility
WMS	Wire mesh sensor
PDF	Probability density function
PSD	Power spectral density

Summary

The GO-VIKING deliverable D4.3 is aimed at providing the experimental configurations of the tests performed by IRSN in the TREFLE facility. The document provides a description of the test setup, boundary conditions, measuring techniques, test parameters. Some results are also provided, however the scope of this deliverable is not to include the comprehensive results, which will be provided in the deliverable D4.4.

Keywords

TREFLE, Flow Test Conditions, WMS, Dual Optical probe.

1. Introduction

The deliverable D4.3 provide an overview of the two-phase TREFLE experiments. The document begins with an introduction to the TREFLE experimental set-up. It then details the various experimental measurements carried out, explaining the specific configurations and methods used. Finally, the paper presents some examples of experimental results obtained from these measurements. The scope of this deliverable is not to include the comprehensive results, which will be provided in the deliverable D4.4

2. Experimental Setup

The experimental were carried out in TREFLE test loop that is operated at IRSN (in Cadarache), the main objective of which is to study the two-phase air-water cross-flow and the associated induced vibrations.

2.1 Test Setup

The experimental loop TREFLE is reported in Figure 1 with the schematic layout and the detailed dimensions of the facility (Spina, 2023). The water comes from the bottom through a divergent section. A honeycomb and a plate structure have been installed inside the divergent section in order to ensure a homogeneous velocity profile at the inlet of the facility. The air is delivered into the facility through a gas injector system. The facility is equipped with several transparent faces in order to allows flow visualization.

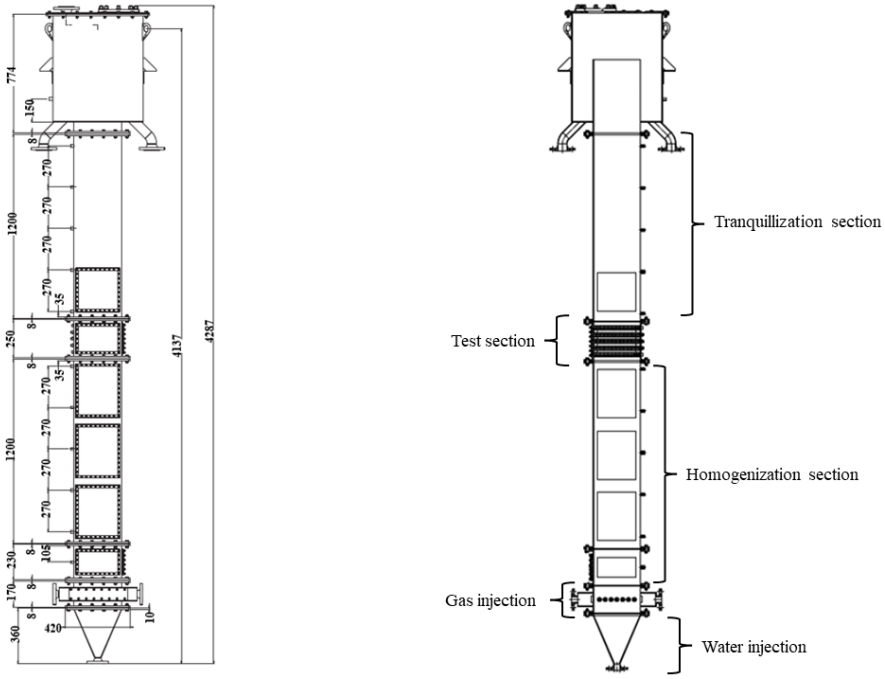

Figure 1: Detailed sketch of the TREFLE facility with dimensions reported in mm.

A homogenization section (about $1400\ \mathrm{mm}$ long) is used in order to make the two-phase flow develop and homogenize before reaching the tube bundle. The test section of the facility contains an in-line, square pitch 5×5 cylinders exposed to an air-water flow. The array, which

features a pitch-to-diameter ratio of 1.44, is composed of relatively large-diameter cylinders (30 mm). This design leads to wider gaps (13.2 mm) between the cylinders (see Figure 2), enabling detailed measurements of the two-phase flow dynamics. The tube length L is 10 times the tube diameter. The tubes can either be fixed or able to vibrate.

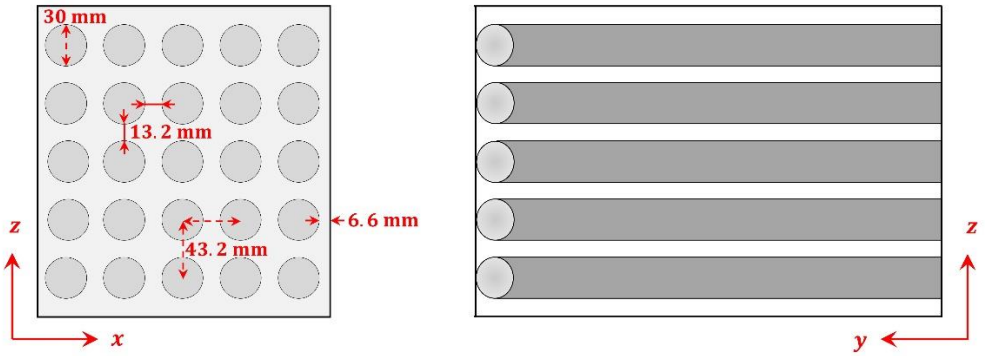

Figure 2: Two side views of the tube bundle section.

The gas injector is designed to be interchangeable (7 injectors), allowing for adapting the component based on the air flow rate. Two types of injectors were utilized in this study: Type 1 for bubbly flow and Type 2 for intermittent flow (see Figure 3).

Figure 3: Two type of air Injector, (a): Type 1 and (b) Type 2.

2.2 Test Initial Conditions

We conducted an experimental investigation by varying the air mass flow rate ($\dot{m}_g$) across a spectrum of 0.5 to 31 g/s while maintaining a consistent water mass flow rate ($\dot{m}_f$) of 2500 g/s, as detailed in Table 1. The experiments included three tests representing a bubbly flow regime (T1, G1 and G2), and three others representing an intermittent flow regime (T5, G3 and G4).

In the case of test T1 and G1, not all the 7 injectors were used, because of the low air mass flow rate: for the test T1, only 2 air injectors were used [Figure 4 (a)] and for test G1 only 5 (Figure 4.b).

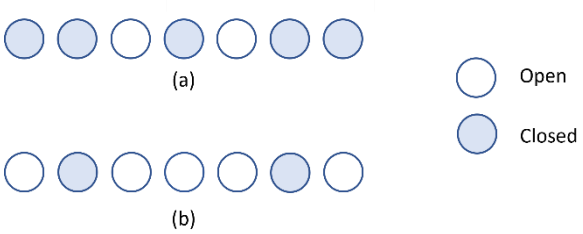

Figure 4: The configurations of the gas injector for the tests (a): T1, and (b): G1.

Test	Number of injector cylinders	Type of tubes	$\dot{m}_f$ [g/s]	$\dot{m}_g$ [g/s]
T1	2	Type 1	2500	0.5
G1	5	Type 1	2500	2
G2	7	Type 1	2500	4.8
T5	7	Type 2	2500	11
G3	7	Type 2	2500	15
G4	7	Type 2	2500	31

Table 1: Summary of the test configurations and initial conditions employed in this study.

2.3 Instrumentation

For this study, precise distribution of void fraction measurement was achieved by employing a wire mesh sensor (WMS) with dimensions measuring $308\ \text{mm} \times 224\ \text{mm}$. The wire mesh of the WMS has a pitch of $4\ \text{mm} \times 3.94\ \text{mm}$ (see Figure 5). The sensor is high resolution and can reach $2500\ \text{Hz}$. Utilising the WMS we can determine the bubbes diameters.

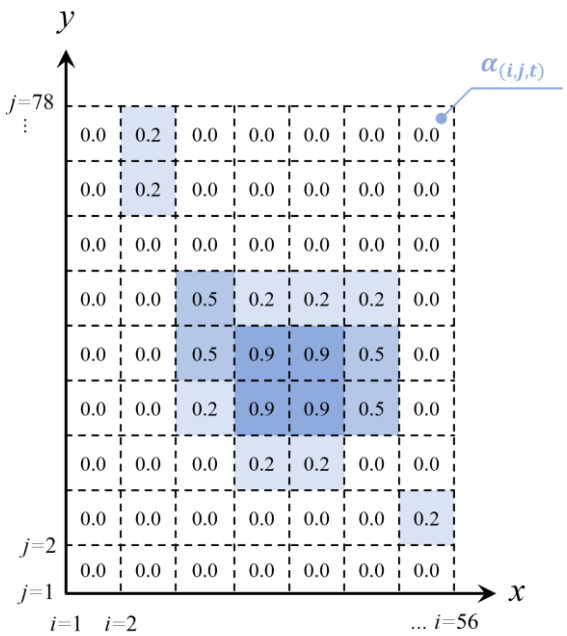

Figure 5: The spatial coordinates within the wire-mesh processing data, along with the representation of the void fraction for individual cells denoted as $\alpha_{(i,j,t)}$.

The second system used was an optical probe. The optical dual tip probe is composed of two sapphire tips ($30\ \mu m$ of diameter) spaced $1.12\ \text{mm}$ apart in the direction of the flow and $0.84\ \text{mm}$ in the direction perpendicular to the flow. The tip details are reported in Figure 6,and the distance between the two tips was measured utilizing an electrical microscope. The dual optic wire is linked to an Opto-Electronic Amplifier from RBI. This amplifier is subsequently connected to a PC responsible for visualization and various calculations, such as void fraction, Sauter diameter, and bubble velocity.

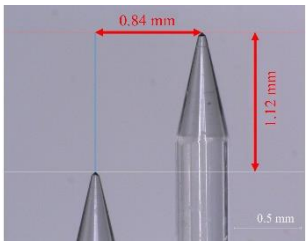

Figure 6: Detail of the optical probe tips.

2.4 Experimental Procedure

2.4.1 WMS measurements

Within the TREFLE facility, the WMS was positioned at two distinct locations: first, $27\ \text{cm}$ upstream of the tube bundle, and second, right after the tube bundle at distance of $3\ \text{cm}$ (see Figure 7). The measurements using the WMS were done over a period of 800 seconds at a frequency of acquisition $1000\ \text{Hz}$.

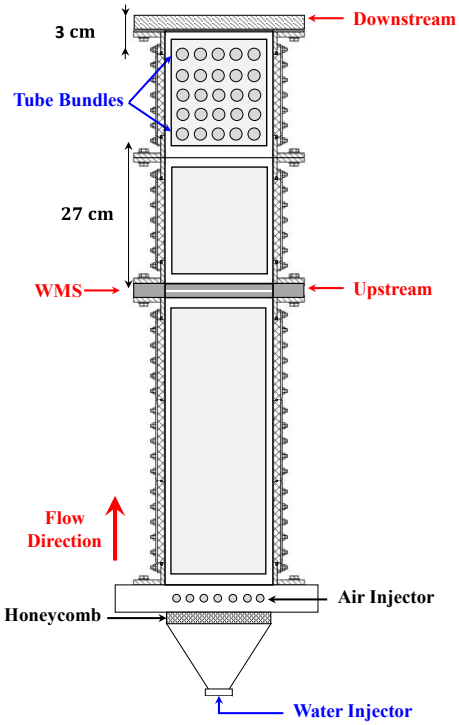

Figure 7: Configuration of TREFLE facility layout and positions of the WMS.

2.4.2 Dual Optical Probe measurements

The dual optic probe was fixed inside the experimental setup at a horizontal position corresponding to the middle of the gap between the 3rd and the 4th columns, as shown in Figure 8. This position corresponds to the coordinates ($\boldsymbol{i = 22, j = 39}$) in the WMS. The measurements were conducted at $\boldsymbol{7}$ distinct vertical positions for each test, and each test repeated four times.

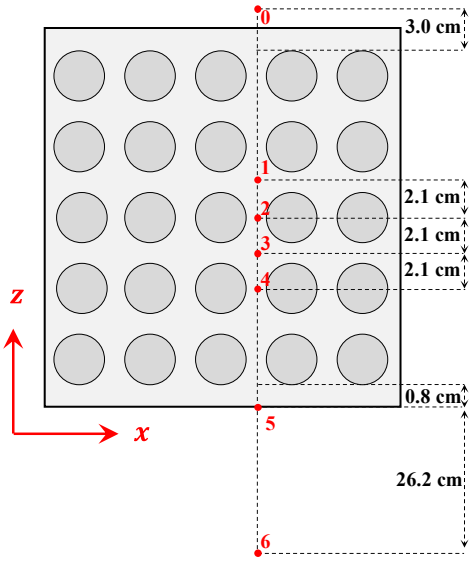

Figure 8: Presentation of the different measurement's points of the dual optical probe.

The measurements were done over a time period of $\boldsymbol{800}$ seconds with a sampling frequency of $\boldsymbol{20\ kHz}$. The positions $\boldsymbol{0}$ and $\boldsymbol{6}$ of the dual optical probe correspond to the positions of the WMS (downstream and upstream of the tube bundle, respectively). This allows to obtain both WMS and optical probe measurements at the same position.

3. Results

3.1 Results of the WMS

The mean void fraction obtained from the WMS at the upstream and downstream positions for all the test conditions provided in Table 1 are presented in Figure 9. Three different flow regimes were distinguished: (1) Bubbly, (2) Transition, and (3) Intermittent.

The void fraction measured downstream of the tube bundle is lower than the one measured upstream of it. This is probably due to the presence of the tube bundle, influencing the two-phase flow.

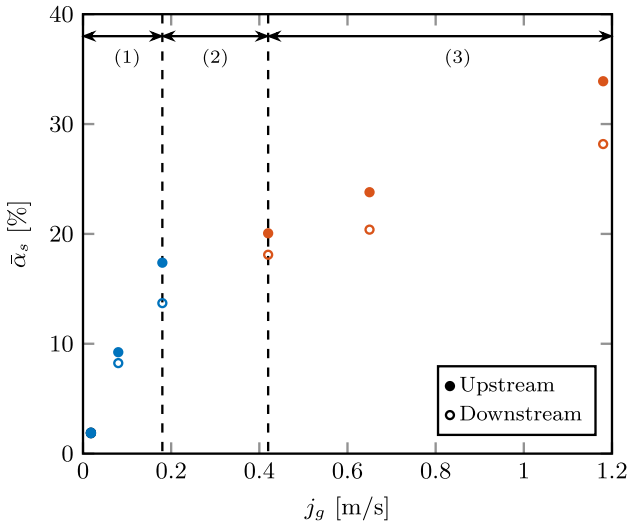

Figure 9: Void fraction variation upstream and downstream of the tube bundle for the different air superficial velocities tested (the water superficial velocity was constant).

3.1.1 Results of WMS at the upstream position

The temporal evolution of the areal void fraction is depicted in Figure 10 for test G1. The graph illustrates the dynamic changes in this parameter for 5 seconds during the experimental process.

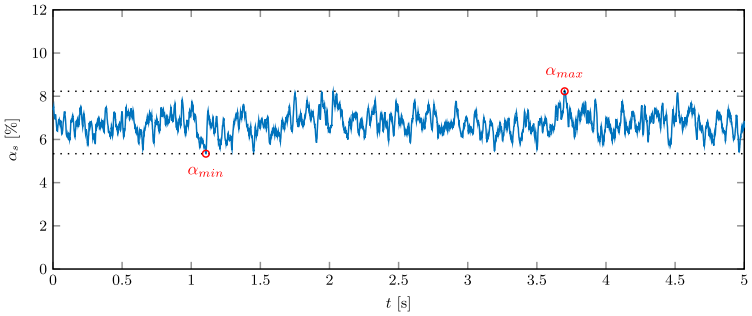

(a)

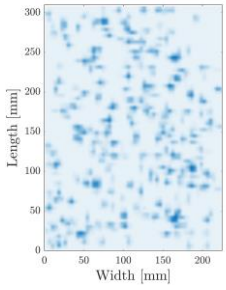

(b) $\alpha_{min} = 5.34$ %

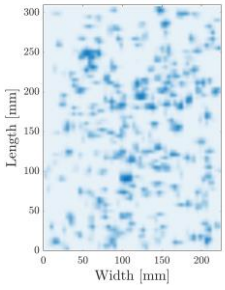

(c) $\alpha_{max} = 8.23$ %

Figure 10: (a) Void fraction evolution over time for Test G1, (b) void fraction distribution at time $t = 1.106$ s and (c) void fraction distribution at time $t = 3.701$ s.

Figure 10 (b, c) illustrates the cross-section at distinct areal void fractions: $\alpha_{min} = 5.34\%$ and $\alpha_{max} = 8.23\ \%$, respectively. This flow is composed of dispersed small gas patches with diameters ranging from 0.8 to $30\ \mathrm{mm}$. The void fraction evolution with time (Figure 10 (a) shows low variation (lower than 3% of void fraction), indicating an overall rather homogeneous shape of the two-phase flow crossing the WMS, typical of bubbly-flow.

The signal displayed in Figure 11 refers to test G3 and exhibits oscillations of $\mathbf{20}\%$ between the lower and higher valuers of void fraction. At its lowest values, the void fraction distribution shows the presence of rather small bubbles (Figure 11 (b)). On the other hand, the highest values of void fractions correspond to the presence of very large gas structures crossing the WMS in the central region (Figure 11 (c)), together with smaller bubbles in the region closer to the walls.

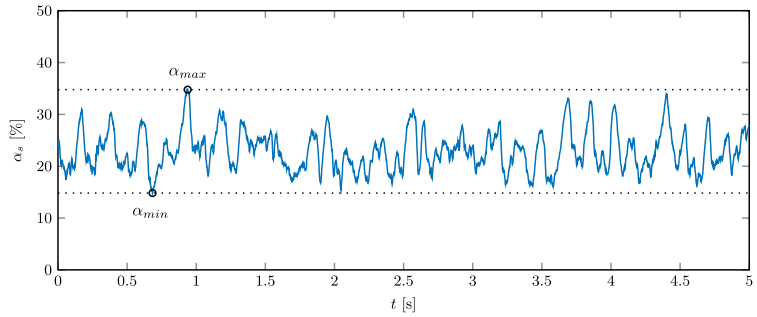

(a)

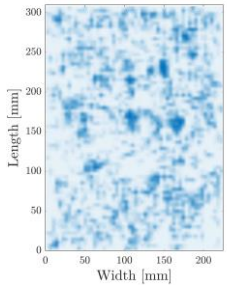

(b) $\alpha_{min} = 14.82\ \%$

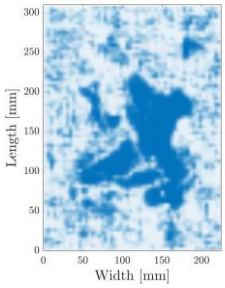

(c) $\alpha_{max} = 34.77\ \%$

Figure 11: (a) Void fraction evolution over time for Test G3, (b) void fraction distribution at time $t = 0.684\ \mathrm{s}$, and (c) void fraction distribution at time $t = 0.938\ \mathrm{s}$.

The probability density functions (PDF) of the void fraction for various tests are depicted in Figure 12. In bubbly flow, the PDF exhibited a narrow width, reflecting minimal variations in the void fraction. In contrast, the intermittent flow exhibits a broader distribution of void fraction values, illustrating the different gas-liquid structures.

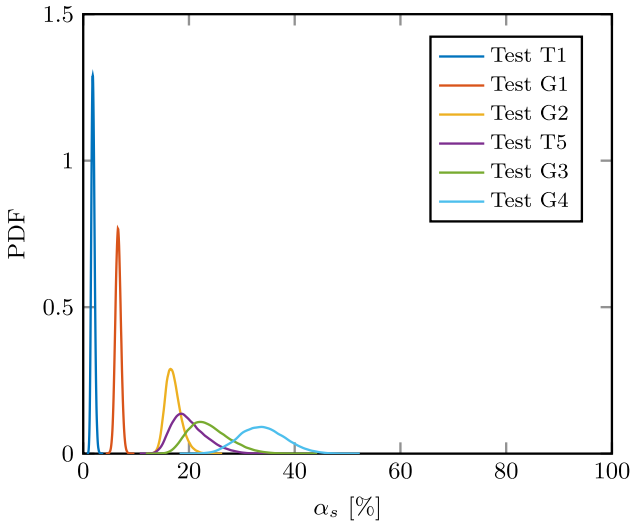

Figure 12: Probability density functions (PDF) representing void fraction for different tests at the upstream positions.

The distribution of the time-averaged void fraction profiles from the center to the wall of the duct (WMS indexes $j = 2, 7, \text{and } 39$), for the tests T1 and G3, along the two horizontal directions x and y, are presented in Figure 13.

For $y = 8$ mm ($j = 2$), the void fraction profile prominently exhibits peaks near the test section's walls. Moving to $y = 28$ mm ($j = 7$), we observe a transition from wall peaking to intermediate void peaking, with the profile indicating a more evenly distributed void fraction between the walls and the core of the test section. At $y = 154$ mm ($j = 39$), the highest void fraction concentrates in the center of the duct section.

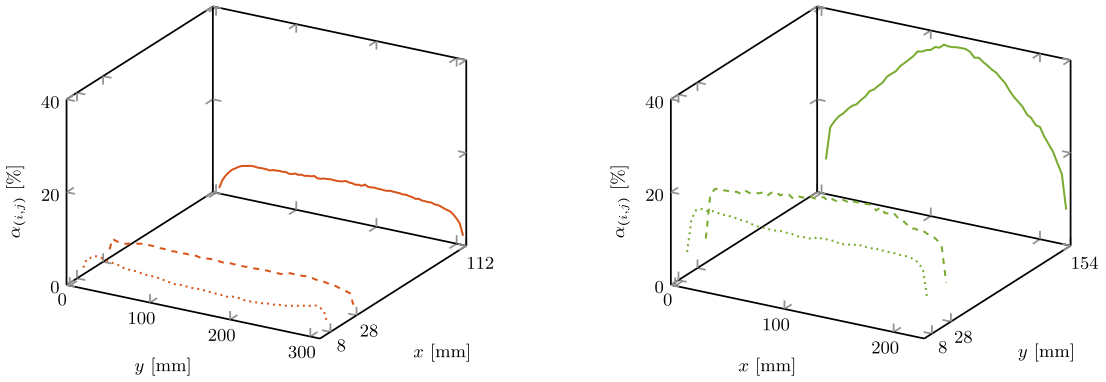

(a) Test G1 **(b) Test G3**

Figure 13: Lateral mean void fraction distribution at three different positions of the vein - upstream position.

The distribution of the time-averaged void fraction at the center of the duct, respectively at $i = 28$ and $j = 39$, is presented for both upstream and downstream positions along both the x and y directions in Figure 14.

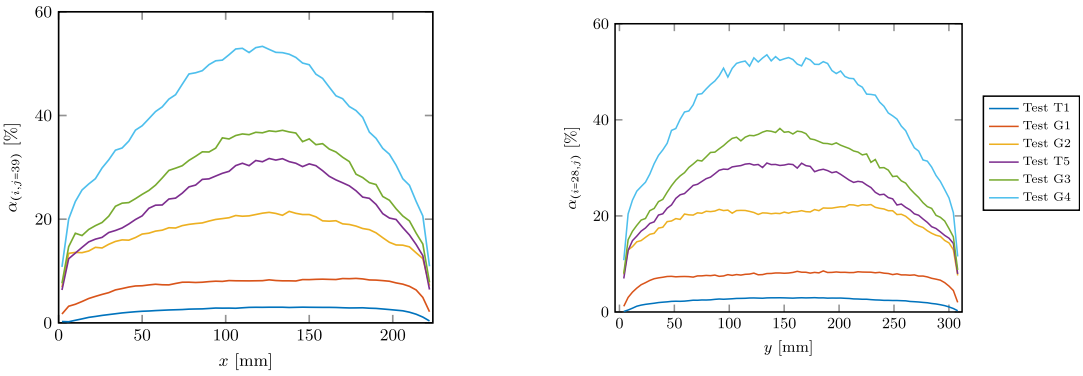

(a) Width direction, $j = 39$ **(b) Length direction, $i = 28$**

Figure 14: Lateral mean void fraction distribution at the center of the duct at the position corresponding to $i = 28$ and $j = 39$ at the upstream position.

By utilizing the void fraction signal obtained from the wire mesh sensor (WMS), we subjected it to power spectral density (PSD) analysis. This analytical approach enabled us to extract valuable insights about the flow's characteristics, including its underlying frequencies (see Figure 15). In Figure 15 (a), which illustrates the bubbly flow regime, the analysis highlights the absence of a distinct frequency distribution linked to the void fraction fluctuations inherent in this flow pattern. A distinct frequency prominently appears in the Power Spectral Density (PSD), approximately at 50 Hz, corresponding to electrical systems.

In contrast, within the intermittent flow regime, the frequency analysis, as depicted in Figure 15 (b), reveals distinct peaks corresponding to the significant bubble structures as they pass through the wire mesh sensor (WMS) in a fraction of a second. The observed peaks were centered at approximately 3 Hz, which indicate the occurrence of three prominent bubble structures passing through in a time of 1 second.

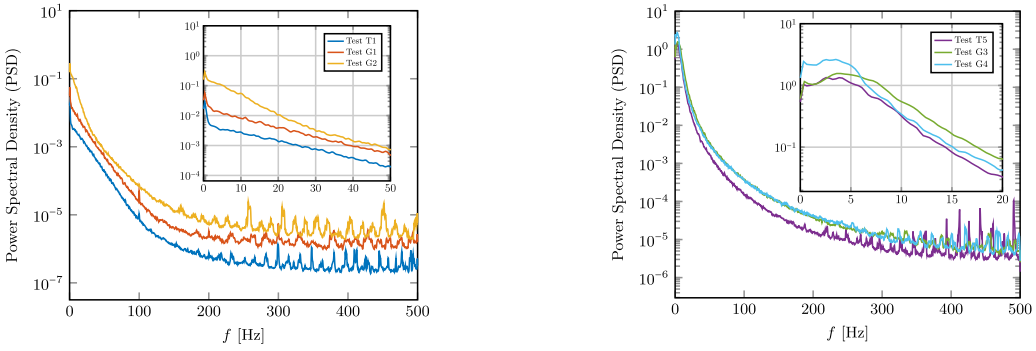

(a) Bubbly flow regime **(b) Intermittent flow regime**

Figure 15: The frequency spectrum of the void fraction for different air velocities at the upstream position.

3.1.2 Results of WMS at the downstream position

The WMS was relocated downstream of the flow, situated 3 cm from the tube bundle. The experiments were conducted under the same test conditions as those used for the upstream

position (see Table 1). The impact of the tube bundle is evident, as indicated by the lower void fraction observed at the downstream position (see Figure 9).

In the context of bubbly flow (test G1), noticeable ripples in the void profile are evident at the downstream location, and these ripples are primarily a result of the positioning of the tubes. This influence is quite pronounced, as depicted in Figure 16 (a). However, when the gas flow increases, these oscillations gradually diminish and disappear (Figure 16 (b)).

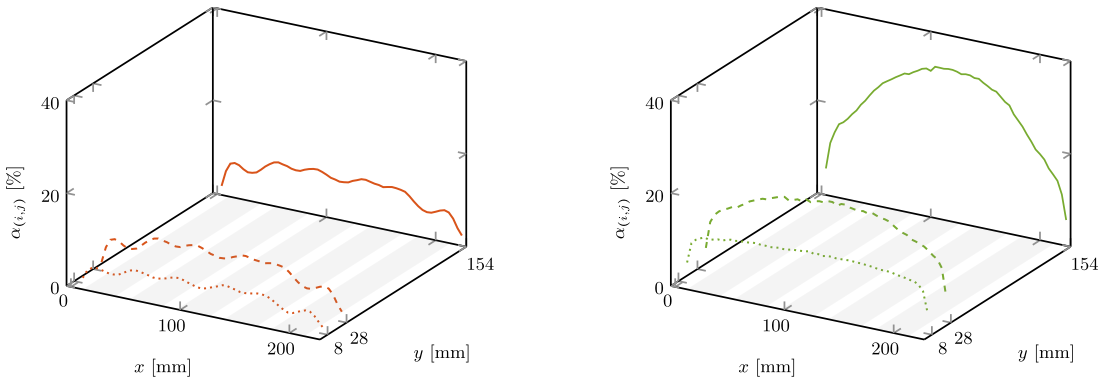

(a) Test G1 **(b) Test G3**

Figure 16: Lateral mean void fraction distribution at three different positions at the downstream position.

Figure 17 presents the time-averaged void profiles in the width direction for $j = 39$ and length direction for $i = 28$, respectively. These profiles provide a detailed representation of how the tube bundle influences the distribution of voids, for both tests T1 and G1. In contrast, for the other tests (G2, T5, G3, and G4), the profile keeps more similar to the corresponding upstream position measurements.

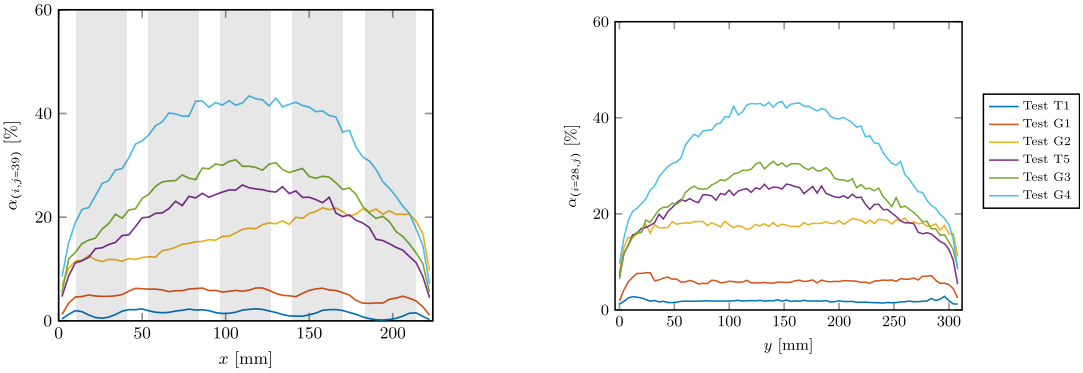

(a) Width direction, $j = 39$ **(b) Length direction, $i = 28$**

Figure 17: Lateral mean void fraction distribution in the center of the duct at the position corresponding to $i = 28$ and $j = 39$, at the downstream position.

The PSD of the void fraction signal at the downstream position is presented in Figure 18. For the intermittent flow regime, the same peak at around 3Hz observed at the upstream position is also found at the downstream position.

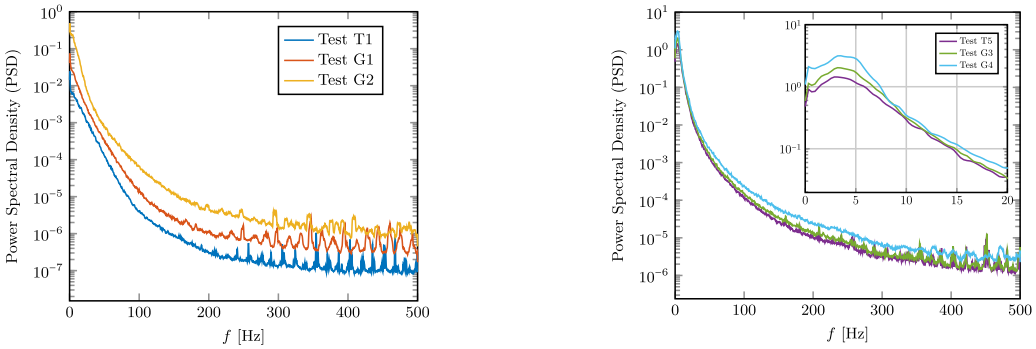

(a) Bubbly flow regime **(b) Intermittent flow regime**

Figure 18: The frequency spectrum of the void fraction for different air velocities at the downstream position.

3.1.3 Comparison of WMS findings between upstream and downstream positions concerning bubble diameter

Using the bubble module, we have determined the bubble characteristics for various tests, as outlined in Table 2 and Table 3 for the upstream and downstream positions respectively. During this analysis, we quantified three parameters: the mean void fraction ($\bar{\alpha}$), the Sauter bubble diameter (d_{32}), and the number of bubbles (N_b), that traversed through the WMS. The characterization process was carried out over a 60-second duration, we repeated the process on three distinct time intervals for each test: $0 - 60$ s, $360 - 420$ s, and $600 - 660$ s, due to the substantial number of bubbles encountered.

Table 2: Experimental results: mean void fraction, Sauter diameter, and the number of bubbles over a 60 second-time interval for different tests (upstream).

	$0 - 60$ s			$360 - 420$ s			$600 - 660$ s		
Test	$\bar{\alpha}$ [%]	d_{32} [mm]	N_b	$\bar{\alpha}$ [%]	d_{32} [mm]	N_b	$\bar{\alpha}$ [%]	d_{32} [mm]	N_b
T1	1.89	4.55	491754	1.89	4.55	491262	1.86	4.55	494152
G1	6.68	5.72	988361	6.66	5.73	987786	6.69	5.72	987668
G2	19.46	8.24	1366465	19.47	8.23	1377871	19.17	8.18	1374862
T5	20.01	8.24	1661502	19.88	8.23	1621920	19.83	8.18	1635754
G3	23.85	8.77	1676835	23.96	8.79	1689828	24.01	8.80	1660618
G4	33.84	9.46	1655820	33.95	8.52	1703628	33.88	8.51	1682127

Table 3: Experimental results: mean void fraction, Sauter diameter, and the number of bubbles over a 60 second-time interval for different tests (downstream).

	$0 - 60$ s			$360 - 420$ s			$600 - 660$ s		
Test	$\bar{\alpha}$ [%]	d_{32} [mm]	N_b	$\bar{\alpha}$ [%]	d_{32} [mm]	N_b	$\bar{\alpha}$ [%]	d_{32} [mm]	N_b
T1	1.90	4.69	433468	1.94	4.69	435633	1.95	4.68	441870
G1	6.30	5.75	894353	6.20	5.73	898554	6.35	5.75	904290
G2	13.77	7.39	1348140	13.87	7.36	1360799	13.78	7.35	1377298
T5	18.12	7.95	1467498	18.00	7.95	1453952	17.78	7.90	1463896
G3	20.70	8.25	1501733	20.32	8.19	1495715	20.24	8.21	1521539
G4	28.26	8.86	1504804	28.13	9.90	1492521	28.55	8.93	1472485

Figure 19 (a-f) displays the probability density functions (PDF) illustrating the bubble diameter (d) for various tests. The solid line represents data from the upstream position, while the dashed line corresponds to the downstream position. We included a magnified version of the original graph in each of the Figure 19 (a-f).

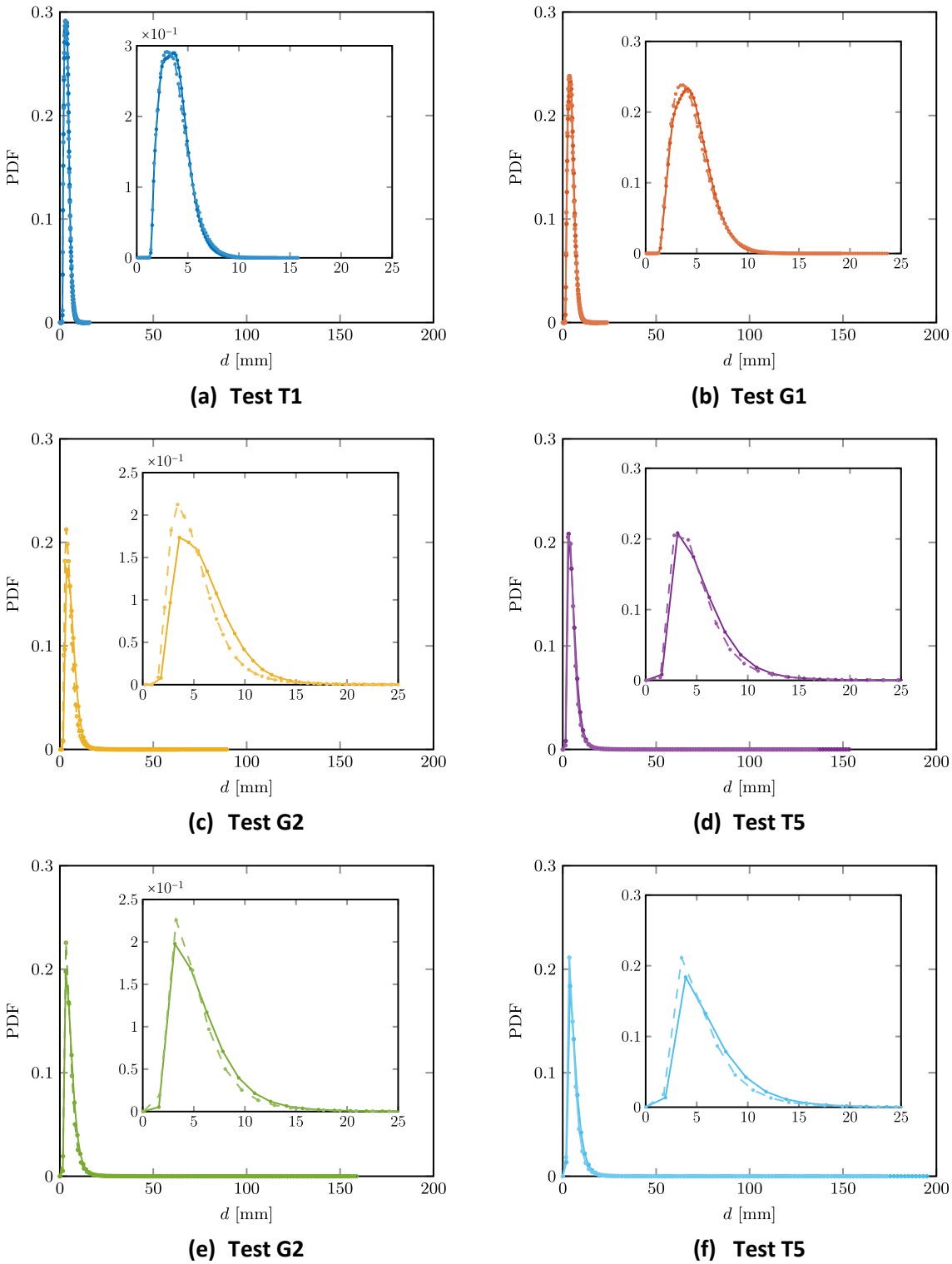

(a) Test T1 (b) Test G1

(c) Test G2 (d) Test T5

(e) Test G2 (f) Test T5

Figure 19: Probability density functions (PDF) representing bubble diameter for different tests for a time interval between 360 and 420 seconds. The solid line corresponds to the upstream, while the dashed line corresponds to the downstream.

In Figure 19 (a, b), that corresponds to a low gas flow velocity featuring bubbly flow, the observed bubble diameters did not exceed 20 mm, with the majority of the observed bubbles

ranging from 1 to 5 mm, as indicated by the plateau-shaped peak in the PDF. As we increased the gas flow velocity, the bubble diameters predominantly fell within the range of 12 mm (see Figure 19 (c, d)). However, a significant change in bubble diameter becomes apparent with a further increase in the gas flow velocity to higher than $j_g = 0.65$ m/s corresponding to intermittent flow conditions. Larger bubbles with maximum diameters of approximately 160 mm are measured, as depicted in Figure 19 (e, f). Here, the PDF displays a sharply pointed peak centered at around 6 mm. This characteristic peak indicates that the majority of the bubbles were tightly clustered around this specific diameter.

The 3D reconstruction of the gas phase evolution at the upstream and downstream positions is presented in Figure 20 (a, b), for test T5. The time dimension, represented by the z-axis, is converted into spatial distance using the bubble velocity measured by a double optical probe placed at the same upstream position of the WMS. The reconstruction suggests the presence of a slightly smaller gas structures at the outlet of the tube bundle, compared to the inlet. This trend was also confirmed by the PDF of the bubble diameters at the two positions (not shown here).

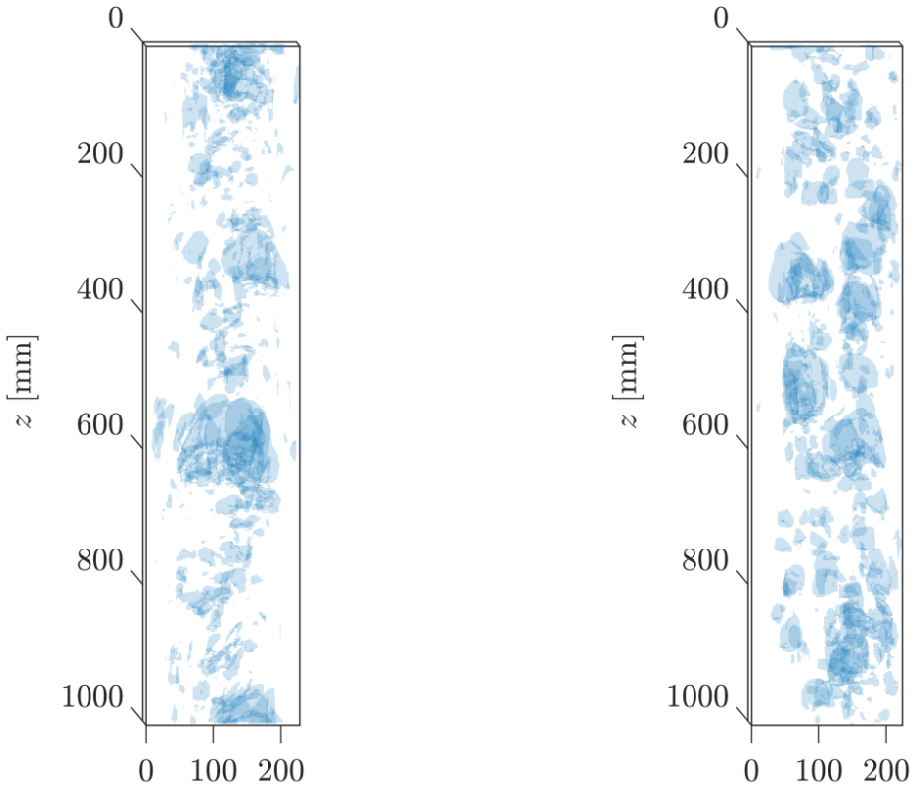

(a) Upstream **(b) Downstream**

Figure 20: Visualization of the bubbles for test T5 at time interval of 360 to 361 second with a time step of 0.001 s.

3.2 Results of the dual optical probe

The dual optic probe was placed inside the experimental section, in the central position shown in Figure 8. The measurements were conducted at the upstream position of the WMS and inside the tube bundle. Each test was repeated 4 times over 800 seconds to ensure convergence of the measurements. Errors arising from the flow measurements did not exceed 15% (see Table 4). At the WMS upstream position, the comparison between results from the WMS and from the optic shows good agreement.

Test	$\overline{\alpha_{OP}}$ [%]	$std(\overline{\alpha_{OP}})$ [%]	$\overline{\alpha_{WMS}}$ [%]
T1	2.8	4	2.75
G1	6.07	15	7.86
G2	17.63	6	19.3
T5	26.92	13	27.56
G3	31.52	13	32.81
G4	43.15	9.5	45.43

Table 4: The void fraction and corresponding error of the measurement using the dual optical probe for different tests at the upstream position (P6).

The time-averaged void fraction values measured at the different positions are presented in Figure 21.

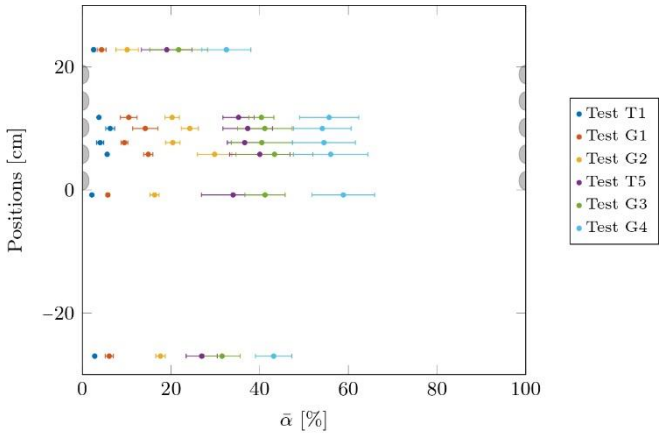

Figure 21: The different mean void fraction and corresponding error at different positions.

The mean gas velocities are determined using the dual optical probe for all the different tests at different positions and are presented in Figure 22.

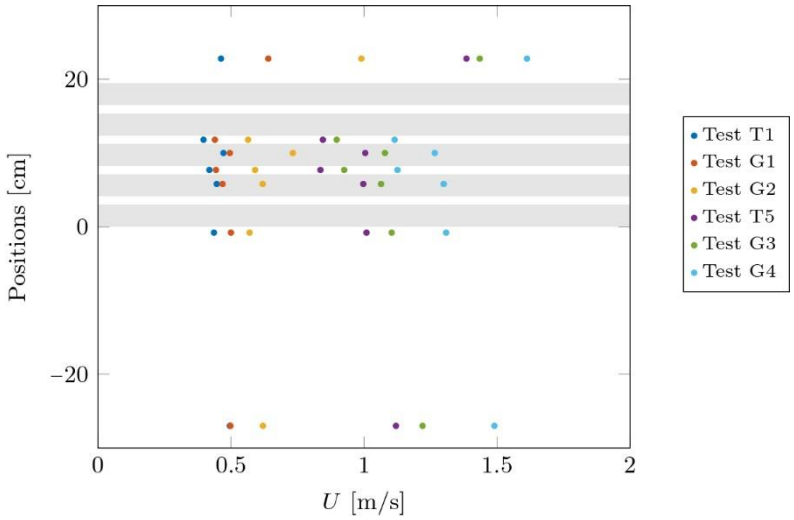

Figure 22: The different mean velocity at different positions.

The Sauter diameter (d_{32}) of bubbles and corresponding error are determined using the dual optical probe for all the different tests at different positions and are presented in Figure 23.

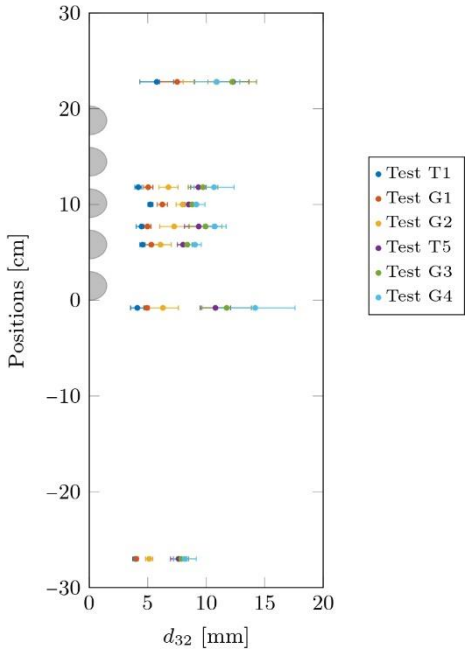

Figure 23: The Sauter diameter at different positions.

4. TREFLE Benchmark

TREFLE experimental tests are planned to be simulated numerically in the frame of WP4. The specific test conditions retained for the simulations are under discussion among the participants.

Conclusion

This document provides a description and the experimental measurement configurations of the TREFLE facility. The two-phase flow is characterized upstream and downstream of the tube bundle using a WMS sensor, and a dual optical probe is used for the measurements inside the tube bundle.

Funded by
the European Union

Bibliography

Spina, G., (2023). Experimental and numerical study of two-phase flows and of fluid-structure interactions inside a cross-flow tube bundle. Ph.D. thesis, INP Toulouse, Toulouse, France.

Funded by
the European Union